ENERGY SURFACES AND HIERARCHIES OF BIFURCATIONS.

Instabilities in the forced truncated NLS.

Eli Shlizerman
Faculty of mathematical and computer science
Weizmann Institute, Rehovot 76100, Israel

Vered Rom-Kedar
Faculty of mathematical and computer science
Weizmann Institute, Rehovot 76100, Israel

Abstract   A two-degrees of freedom near integrable Hamiltonian which arises in the study of low-amplitude near-resonance envelope solutions of the forced Sine-Gordon equation is analyzed. The energy momentum bifurcation diagrams and the Fomenko graphs are constructed and reveal the bifurcation values at which the lower dimensional model exhibits instabilities and non-regular orbits of a new type. Furthermore, this study leads to some new insights regarding the *hierarchy of bifurcations* appearing in integrable Hamiltonian systems and the role of global bifurcations in the energy momentum bifurcation diagrams.

1.   Introduction

Despite a century long study of near integrable Hamiltonian systems, our qualitative understanding of inherently higher dimensional (non-reducible to smooth symplectic two dimensional maps) dynamics is lacking. Recently we proposed a framework for obtaining such qualitative information for a class of near-integrable Hamiltonian systems [25, 26, 27]. Here we provide a first example of a physical system which is studied using this framework, demonstrating that some new insights are gained regarding the physics and adding some new ingredients to the general framework which is still under construction.

Qualitative understanding means here that the effect of small perturbations on different unperturbed orbits may be a-priori predicted for some non-trivial time scales. For example, such a qualitative understanding exists for generic near integrable one-and-a half degrees of freedom systems; We know that for such systems most of the phase space will be filled by KAM tori, KAM Cantori and resonance bands whereas homoclinic loops of the integrable system will create homoclinic chaotic zones. While there are some long standing open problems regarding the asymptotic behavior of such systems (notably the decay rate of averaged observables in the chaotic zone and the measure of the chaotic zone [20, 36]), the basic transport and instability mechanisms are well understood on time scales which are logarithmic in the perturbation parameter [29, 33]. Another example is the behavior of orbits of near-integrable n degrees of freedom systems in a neighborhood of an unperturbed compact regular non-degenerate level set with Diophantine frequency vector; While the asymptotic behavior of the solutions in such regions is still unknown (the famous Arnold diffusion conjecture addresses this question), it is known that for extremely long time (at least exponential in the perturbation parameter [31, 15]) the orbits will hover near the preserved KAM tori. In both examples, while the asymptotic behavior is unknown, there is a good understanding of the characteristic behavior of all orbits in a given neighborhood for a long transient time.

Recently it has been proposed that a similar qualitative understanding of the behavior of orbits near non-regular level sets in some higher dimensional systems may be achieved by studying the structure of the energy surfaces and their bifurcations using the energy momentum bifurcation diagrams and branched surfaces (see [25, 26, 27] and references therein, including the important previous works [35, 24, 13, 12]). So far, this theory was applied to Hamiltonian systems which are polynomial in their arguments and are built to satisfy some specific bifurcation scenarios via a normal-form type of construction ([25, 26, 27]). In particular, for all these examples, the unperturbed energy surface topology and the foliation of the level sets on them were trivial. In general, the classification of all possible topologies and level sets foliations of an energy surface of integrable systems is unknown: it had been completed for the two degrees of freedom case [14, 24], whereas in higher dimensions even the characterization of specific systems like the Lagrange top turns out to be extremely difficult (see [14, 12, 23] and references therein). Here we apply the general framework of ([25, 26, 27]) to equations which have not been previously analyzed from this point of view - a truncated two mode model of the perturbed Sine-Gordon equation. This is a two-degrees-of-freedom model, and, as expected, no new topological structure of the

energy surfaces are discovered. However, a comprehensive way of studying the dependence of these structures on the energy level and on the parameters is presented, leading to identifying new dynamically interesting regimes.

This reduced model was suggested by Bishop et al. and collaborators [4, 2, 8, 5, 3, 6, 7, 11] who investigated analytically and numerically the damped and driven Sine-Gordon equation. Their numerical studies have revealed chaotic behavior and the existence of low dimensional chaotic attractors of the PDE. Using the near resonance envelope expansion for the Sine-Gordon model they have transformed the problem to the investigation of the perturbed NLS model. Introducing a two-mode symmetric Galerkin approximation for the solutions of the perturbed NLS they have derived the corresponding truncated equations for the complex amplitudes. Finally, they have shown that the unperturbed truncated system is a two degrees of freedom Hamiltonian system with an additional integral of motion, and, hence, is integrable. They found numerically that in some parameter regime this low dimensional model supplies qualitative behavior which is similar to the observed behavior of the PDE. Investigation of the truncated system lead to the discovery of a new mechanism of instability - the hyperbolic resonance - by which homoclinic solutions to a lower dimensional resonance zone are created [22, 16, 19, 18]. The unperturbed structure of the truncated model which is responsible to this behavior is a circle of fixed points which is hyperbolic in the transverse direction (see section 3 for a precise definition). New methodologies and tools introduced to this PDE-ODE study have finally lead to a proof that the homoclinic resonance dynamics, and in particular the birth of new types of multi-pulse homoclinic orbits which is associated with it, has analogous behavior in the PDE setting (see [17, 11, 28] and references therein).

The appearance of a hyperbolic circle of fixed points in the truncated model is not a special property of the NLS model - investigation of the structure of low-dimensional near-integrable Hamiltonian systems (see [26]) shows that hyperbolic resonances are persistent[1] phenomenon in n degrees of freedom systems with $n \geq 2$; Among such integrable Hamiltonian systems there are open sets of Hamiltonians which have an $n - 1$ dimensional torus of fixed points which is normally hyperbolic. Furthermore, it is established that parabolic resonant tori (here, the ap-

---

[1]The existence of such tori may be formulated as the existence of transverse intersection of some finite dimensional manifolds. Hence, using the Transversality theorem, one proves that hyperbolic resonant tori exist for a C^1-open set of integrable Hamiltonians, which we take hereafter as the definition of persistence.

pearance of an unperturbed circle of fixed points which are parabolic in the transverse direction, more details appear in section 3) are persistent in families of near-integrable Hamiltonians if $n + p > 2$ where n is the number of the degrees of freedom and p is the number of the control parameters [26]. Hence, including one parameter in a two degrees of freedom model naturally leads to a persistent appearance of a parabolic resonance. The truncated NLS model depends on one parameter - the dimensionless wave number of the first symmetric mode. We show that as this parameter is varied, parabolic resonant tori are created. In fact, we are able to provide a complete and novel description of the structure of the energy surfaces as a function of the energy and the parameter, discovering two phenomena which have not been observed nor analyzed yet for this model - the appearance of parabolic resonances and the appearance of resonant global bifurcation. Furthermore, since under conservative perturbations, the solutions remain on a given energy surface, our characterization supplies a priori bounds to the perturbed motion.

The paper is organized as follows. In the second section we present the derivation of the truncated model of the NLS (following [4, 22]). In section 3 we describe the structure of regular and singular level sets for a general integrable Hamiltonian (following [27]). We use the truncated NLS model as a particular example for the theory, and describe the structure of the energy surfaces for this model using the EMBD and the Fomenko graphs. The fourth section lists the hierarchy of bifurcations in general and for the truncated model in particular, finding the energy bifurcating values, their bifurcation diagram and the dynamical significance of these bifurcations. We present a few simulations showing the instabilities encountered at such bifurcation values. The short discussion is followed by appendix A, where we prove that the energy surfaces of this model are bounded and that the perturbed surfaces are close to the unperturbed surfaces. Appendix B includes the energy-momentum bifurcations diagrams and Fomenko graphs for several parameter values.

2.   The two-mode truncation model of the perturbed NLS

Here we recall the relevant results of Bishop et al. [4, 2, 8, 5, 3, 6, 7] followed by Kovacic and Haller [22, 16, 19, 18, 17] results who developed the two-mode truncation model and studied some of its features. Bishop et al. investigated the chaotic attractor of the damped driven Sine-Gordon Equation (SGE) with even spatial symmetry and periodic boundary conditions:

$$u_{tt} - u_{xx} + \sin u = \delta(-\hat{\alpha}u_t + \hat{\Lambda}u_{txx} + \hat{\Gamma}\cos(\omega t)), \tag{1}$$
$$u(x) = u(x+L), \ u_x(0) = 0.$$

ω is the driving frequency, L is the box size, $\delta\hat{\Gamma}$ is the driving amplitude, $\delta\hat{\alpha}$ is the damping and $\delta\hat{\Lambda}$ is an additional wave-number dependent damping term which was introduced in [22]. The NLS approximation for the SGE is obtained by developing a small amplitude envelope approximation for the near resonance frequency ($\omega = 1 - \delta\tilde{\omega}$) case. More precisely, one looks for solutions of the SGE of the form:

$$u = 2\sqrt{\delta\tilde{\omega}}[B_\delta(X,T)e^{i\omega t} + B_\delta(X,T)^* e^{-i\omega t}], \tag{2}$$

where $B_\delta(X,T)$ is assumed to be analytic in δ, and

$$\omega = 1 - \delta\tilde{\omega}, \ \ X = \sqrt{2\delta\tilde{\omega}}\ x, \ \ T = \delta\tilde{\omega}t.$$

Introducing a small parameter ε such that

$$\hat{\Lambda} = \varepsilon\Lambda, \ \ \hat{\Gamma} = \varepsilon 8\delta^{3/2}\tilde{\omega}^{3/2}\Gamma, \ \ \hat{\alpha} = \varepsilon 2\tilde{\omega}\alpha,$$

with all other parameters of order one, one finds that provided[2]

$$\delta \ll \varepsilon \ll 1$$

the leading order term in δ, $B(X,T) = B_0(X,T)$, satisfies the following forced and damped NLS equation:

$$-iB_T + B_{XX} + (|B|^2 - 1)B = i\varepsilon(\alpha B - \Lambda B_{XX} + \Gamma). \tag{3}$$

Consider a two mode complex Fourier truncation for equation (3):

$$B(X,T) = \frac{1}{\sqrt{2}}c(T) + b(T)\cos kX. \tag{4}$$

The periodic boundary conditions imply that

$$k = \frac{2\pi}{\sqrt{2\delta\tilde{\omega}}L}n, \ \ n \in Z_+. \tag{5}$$

By substituting this solution to the NLS equation and neglecting (see [4, 2, 8, 5, 3, 6, 7, 11] for discussion of this step) higher Fourier modes, one obtains the following two ODE's:

---

[2]This consistency conditions has not been set explicitly in previous publications.

$$-i\dot{c} + (\frac{1}{2}|c|^2 + \frac{1}{2}|b|^2 - 1)c + \frac{1}{2}(cb^* + bc^*)b = i\varepsilon(\alpha c + \sqrt{2}\Gamma)$$

$$-i\dot{b} + [\frac{1}{2}|c|^2 + \frac{3}{4}|b|^2 - (1 + k^2)]b + \frac{1}{2}(bc^* + cb^*)c = i\varepsilon\beta b$$

where

$$\beta = \alpha + \Lambda k^2.$$

By setting $\alpha = \Lambda = 0$, one discovers that this is a two d.o.f. Hamiltonian system, which, at $\Gamma = 0$ possesses two integrals:

$$I = \frac{1}{2}(|c|^2 + |b|^2),$$

$$H = \frac{1}{8}|c|^4 + \frac{1}{2}|b|^2|c|^2 + \frac{3}{16}|b|^4 - \frac{1}{2}(1 + k^2)|b|^2 - \frac{1}{2}|c|^2 + \frac{1}{8}(b^2 c^{*2} + b^{*2}c^2).$$

hence, at $\varepsilon = 0$ the system is integrable. The Hamiltonian part of the perturbation is:

$$H_1 = -i\frac{\varepsilon}{\sqrt{2}}\Gamma(c - c^*).$$

Introducing generalized action angle coordinates (x, y, I, γ) [22] (see next section for more details):

$$c = \sqrt{2I - x^2 - y^2}\exp(i\gamma),$$
$$b = (x + iy)\exp(i\gamma)$$

Kovacic and Haller [22, 16, 19, 18, 17] have investigated the corresponding two d.o.f. system. In particular, they have realized that a specially interesting phenomena occurs when the circle $b = 0$ is a normally hyperbolic circle of fixed points (this occurs for $k < \sqrt{2}$ at $I = 1$, see next section for details). Then, at $\varepsilon = 0$, pairs of fixed points on this circle are connected by heteroclinic orbits. This realization lead to a beautiful theoretical study of the behavior of integrable systems with such a normally hyperbolic circle of fixed points under conservative [19, 18, 17] and dissipative [22, 16] perturbations.

Kovacic [22] includes in his study global analysis of the integrable system in which, after identifying the critical I values, the level sets $H = h$ are plotted for typical values of I. We present the integrable system using Energy momentum bifurcation diagrams and Fomenko graphs, which corresponds to investigating the surfaces $H = h$ and their extent in the I direction. We propose that these representation are more adequate for understanding the behavior under small perturbations since the total energy H is preserved (for $\alpha = 0$).

3. Level sets and energy surfaces structure

The structure of energy surfaces and level sets for n degrees of freedom integrable Hamiltonian systems in general (following the formulation of [27]) and their structure for the two mode truncation of the conservatively perturbed NLS in particular are now described. Consider a near integrable Hamiltonian $H(q,p;\varepsilon) = H_0(q,p) + \varepsilon H_1(q,p;\varepsilon)$, $\varepsilon \ll 1$, $(q,p) \in M \subseteq \mathbb{R}^n \times \mathbb{R}^n$, where M is a $2n$-dimensional, analytic symplectic manifold and H_0 and H_1 are[3] C^∞ and H_1 and its derivatives are bounded. H_0 represents the completely integrable part of the Hamiltonian (the unperturbed system) and its structure is described below. For any ε, a perturbed orbit with energy h resides on the energy surface $H_0(\cdot) = h - \varepsilon H_1(\cdot;\varepsilon)$. Hence, by assumption, the structure of the unperturbed energy surfaces and their resonance webs in an $O(\varepsilon)$-interval of energies near h supplies global information on the allowed range of motion of the perturbed orbits (see below for a more precise formulation).

The two mode truncation of the conservatively perturbed NLS (hereafter, since only Hamiltonian perturbations are considered, we set $\bar{\varepsilon} = \varepsilon\Gamma$ and drop the over bar):

$$-i\dot{c} + \left(\frac{1}{2}|c|^2 + \frac{1}{2}|b|^2 - 1\right)c + \frac{1}{2}(cb^* + bc^*)b = i\sqrt{2}\varepsilon \quad (6)$$

$$-i\dot{b} + \left(\frac{1}{2}|c|^2 + \frac{3}{4}|b|^2 - (1 + k^2)\right)b + \frac{1}{2}(bc^* + cb^*)c = 0.$$

where $|b|$ is the amplitude of the first symmetric mode and $|c|$ is the amplitude of the plane wave, is a two degrees of freedom near integrable Hamiltonian of the form:

$$H(c,c^*,b,b^*;\varepsilon) = H_0(c,c^*,b,b^*) + \varepsilon H_1(c,c^*,b,b^*) \quad (7)$$

with the Poisson brackets $\{f,g\} = -2i < \frac{\partial}{\partial c}, \frac{\partial}{\partial c^*} >$, where

$$H_0 = \frac{1}{8}|c|^4 + \frac{1}{2}|b|^2|c|^2 + \frac{3}{16}|b|^4 - \frac{1}{2}(1 + k^2)|b|^2 - \frac{1}{2}|c|^2 + \frac{1}{8}(b^2c^{*2} + b^{*2}c^2).$$
$$(8)$$

$$H_1 = -\frac{i}{\sqrt{2}}(c - c^*). \quad (9)$$

At $\varepsilon = 0$ the system is integrable, having the second integral of motion:

$$I = \frac{1}{2}(|c|^2 + |b|^2).$$

---

[3]One may relax these requirements to the C^r case, but this is left for future studies.

It can be shown that the unperturbed energy surfaces are bounded (see appendix A), and that the perturbed and unperturbed energy surfaces are close to each other as long as the level sets belonging to the unperturbed energy surface are bounded away from neighborhoods of fixed points, so $\|\nabla H_0\| > const \gg \varepsilon$. More precisely, using the implicit function theorem (see appendix), it can be shown that under these conditions any $c^\varepsilon(h^\varepsilon), b^\varepsilon(h^\varepsilon)$ satisfying $H(c^\varepsilon(h^\varepsilon), c^{\varepsilon*}(h^\varepsilon), b^\varepsilon(h^\varepsilon), b^{\varepsilon*}(h^\varepsilon); \varepsilon) = h^\varepsilon = h + O(\varepsilon)$ are $\varepsilon-$close to $c^0(h), b^0(h)$ values. Since there are a finite number of fixed points of the system (6) and these appear at bounded energy values (see appendix), one can conclude that for most part of phase space the unperturbed and perturbed surfaces are close to each other and that the behavior near fixed points requires further analysis, as expected (roughly, if higher order derivatives of order m are non-singular one expects that the perturbed surfaces are order $\varepsilon^{1/m}$ close to the unperturbed ones). Notice that the closeness of the perturbed and unperturbed energy surfaces does not imply that they are topologically conjugate - counter examples may be easily constructed. Nonetheless, this closeness is sufficient to obtain a-priori bounds on the motion.

The integrable n d.o.f. Hamiltonian, $H_0(q, p)$; $(q, p) \in M \subseteq \mathbb{R}^n \times \mathbb{R}^n$, has n integrals of motion: $H_0 = F_1, F_2, ..., F_n \in C^\infty(M)$, which are functionally independent at almost all points of M and are pair wise in involution: $\{F_i, F_j\} = 0$; $i, j = 1, ...n$. For simplicity, we assume that the Hamiltonian level sets, $M_g = \{(q, p) \in M, \quad F_i = g_i; \quad i = 1, ..., n\}$, are compact, so that the integrals of motion are complete. Here, the two integrals of motion are H_0 and I and since the level sets of I are $3-$spheres the Hamiltonian level sets M_g are clearly compact. By the Liouville-Arnold theorem (see [30] and [1, 21]), the connected compact components of the level sets M_g, on which all of the dF_i are (point wise) linearly independent, are diffeomorphic to n-tori and hence a transformation to action-angle coordinates ($H_0 = H_0(J)$) near such level sets is non singular. Here,

$$dI = \frac{1}{2}(c^*, c, b^*, b)$$

$$dH_0 = \begin{pmatrix} c^*(\frac{1}{4}|c|^2 + \frac{1}{2}|b|^2 - \frac{1}{2}) + \frac{1}{4}b^{*2}c) \\ c(\frac{1}{4}|c|^2 + \frac{1}{2}|b|^2 - \frac{1}{2}) + \frac{1}{4}b^2c^* \\ b^*(\frac{1}{2}|c|^2 + \frac{3}{8}|b|^2 - \frac{1}{2}(1 + k^2)) + \frac{1}{4}bc^{*2} \\ b(\frac{1}{2}|c|^2 + \frac{3}{8}|b|^2 - \frac{1}{2}(1 + k^2)) + \frac{1}{4}b^*c^2 \end{pmatrix}$$

thus these are linearly independent for most values of c and b. The values at which dI and dH_0 are linearly dependent (e.g. the plane $c = 0$) are discussed next.

Consider a neighborhood of a level set M_{g0} which possibly contains a singularity set at which the rank of the dF_i's is $n-1$ (here, dI and dH_0 are linearly dependent, but do not vanish simultaneously, so the origin is excluded). Then, on each connected and closed component of such a Hamiltonian level set there is some neighborhood D, in which the Hamiltonian $H_0(q,p)$ may be transformed by the reduction procedure to the form (see [24], [30]):

$$H_0(\bar{q}, \bar{p}, J), \qquad (\bar{q}, \bar{p}, \phi, J) \in U \subseteq \mathbb{R}^1 \times \mathbb{R}^1 \times \mathbb{T}^{n-1} \times \mathbb{R}^{n-1} \quad (10)$$

which does not depend on the angles of the tori, ϕ. The symplectic structure of the new integrable Hamiltonian (10) is $d\bar{q} \wedge d\bar{p} + \sum_{i=1}^{n-1} d\phi_i \wedge dJ_i$, where $(\bar{q}, \bar{p}, \phi, J)$ are the generalized action-angle variables. The motion on the $(n-1)$ dimensional family (parameterized by the actions J) of $(n-1)$-tori is described by the equations:

$$\frac{d\phi_i}{dt} = \omega_i(\bar{q}, \bar{p}, J), \quad \frac{dJ_i}{dt} = 0.$$

The geometrical structure of the new Hamiltonian, $H_0(\bar{q}, \bar{p}, J)$, is such that for any fixed J ($J = (J_1, ..., J_{n-1})$) an $(n-1)$-torus is attached to every point of the $(\bar{q}, \bar{p})$ plane. The $(\bar{q}, \bar{p})$ plane is called the *normal plane* [1, 32, 9] of the $(n-1)$-tori, and defines their stability type in the normal direction to the *family*[4] of tori.

For our example, the transformation to the generalized action angle co-ordinates for $c \neq 0$ was found in Kovacic [22]; taking

$$c = |c| \exp(i\gamma), \quad b = (x + iy) \exp(i\gamma)$$

so that

$$I = \frac{1}{2}(|c|^2 + x^2 + y^2)$$

one obtains the generalized action angle canonical coordinates for the Hamiltonian:

$$H(x, y, I, \gamma) = H_0(x, y, I) + \varepsilon H_1(x, y, I, \gamma),$$

where

$$(I, \gamma) \in (R^+ \times T), \ (x, y) \in B_I = \{(x, y) | x^2 + y^2 < 2I\}$$

---

[4]Notice that a single torus belonging to this family has neutral stability in the actions directions. The normal stability referred to in the Hamiltonian context ignores these directions, see [10, 9] and references therein.

and

$$H_0(x, y, I) = \frac{1}{2}I^2 - I + (I - \frac{1}{2}k^2)x^2 - \frac{7}{16}x^4 - \frac{3}{8}x^2y^2 + \frac{1}{16}y^4 - \frac{1}{2}k^2y^2,$$
(11)

$$H_1(x, y, I, \gamma) = \sqrt{2}\sqrt{2I - x^2 - y^2}\sin\gamma.$$
(12)

The transformation to these variables is singular at $c = 0$, namely on the circle $2I = x^2 + y^2$, where the phase γ is ill defined and the perturbation term has a singular derivative. In Kovacic and Haller [22, 16, 19, 18] the analysis was performed for phase space regions which are bounded away from this circle. Here we would like to include some information regarding the dynamics near this circle as well. We thus use a similar transformation which is valid as long as $b \neq 0$:

$$b = |b|e^{i\theta} \ , \ c = (u + iv)e^{i\theta} \ , \ I = \frac{1}{2}(u^2 + v^2 + |b|^2)$$

and obtain the equation of motion in the canonical coordinates (u, v, I, θ) from the Hamiltonian:

$$H_0(u, v, I) = \frac{3}{4}I^2 + \left(-1 + \frac{3}{4}u^2 - \frac{1}{4}v^2 - k^2\right)I - \frac{7}{16}u^4 - \frac{3}{8}u^2v^2$$
$$+ \frac{1}{2}k^2u^2 + \frac{1}{2}k^2v^2 + \frac{1}{16}v^4$$
$$H_1(u, v, I) = \sqrt{2}(v\cos\theta + u\sin\theta).$$

When both γ and θ are well defined, namely for $cb \neq 0$, the two sets of coordinates are simply related:

$$x = |b|\cos(\theta - \gamma) \qquad\qquad y = |b|\sin(\theta - \gamma)$$
$$u = \frac{|c|}{|b|}x, \qquad\qquad v = -\frac{|c|}{|b|}y.$$

It follows that for $x^2 + y^2 < 2I$ we have:

$$\frac{d\gamma}{dt} = \omega(x, y, I) = I - 1 + x^2 = \frac{\partial H_0(x, y, I)}{\partial I}$$
(13)

and for $u^2 + v^2 < 2I$ we have:

$$\frac{d\theta}{dt} = \omega(u, v, I) = \frac{3}{2}I - 1 + \frac{3}{4}u^2 - \frac{1}{4}v^2 - k^2 = \frac{\partial H_0(u, v, I)}{\partial I}.$$
(14)

Consider now lower dimensional invariant tori which correspond to isolated fixed point(s) of the normal plane. These appear on an $n - 1$

dimensional manifold of J values, the singularity manifold. Locally, one may choose the $(\overline{q}, \overline{p}, J)$ coordinate system so that for these tori:

$$\nabla_{(\overline{q},\overline{p})} H_0(\overline{q},\overline{p}, J)\big|_{p_f} = 0, \qquad p_f = (\overline{q}_f, \overline{p}_f, J_f). \qquad (15)$$

For our example, there are six families of such tori as listed in the following table:

Invariant circle: $\qquad\qquad \theta, \gamma \in T^1$	Exists For	Description
1. $p_{pw} = (x = 0, y = 0, I, \gamma),$	$I \geq 0$	Plane wave $(b = 0)$
2. $p_{sm} = (u = 0, v = 0, I, \theta),$	$I \geq 0$	Symmetric mode $(c = 0)$
3. $p_{pwm}^{\pm} = (x = \pm\sqrt{\frac{4}{7}(-k^2 + 2I)}, y = 0, I, \gamma),$	$I \geq \frac{1}{2}k^2$	PW mixed mode $(bc \neq 0)$
$\quad = (u = \pm\sqrt{\frac{6}{7}I + \frac{4}{7}k^2}, v = 0, I, \theta),$	$I > \frac{1}{2}k^2$	"
4. $p_{smm}^{\pm} = (x = 0, y = \pm 2k, I, \gamma),$	$I > 2k^2$	SM mixed mode $(bc \neq 0)$
$\quad = (u = 0, v = \pm\sqrt{2I - 4k^2}, I, \theta),$	$I \geq 2k^2$	"

Table 1

Following [24] terminology, the invariant tori on which equation (15) is satisfied are called here singular tori and the surfaces of energy and action values on which this equation is satisfied are called singularity surfaces. We will see that the structure of these singularity surfaces serves as an organizing skeleton of the energy surfaces.

The invariant $(n-1)$-tori have an $(n-1)$-dimensional vector of inner frequencies, $\dot{\theta} = \omega(p_f) = \frac{\partial H_0(p_f)}{\partial J}$. The normal stability type of such families of $(n-1)$-tori is determined by the characteristic eigenvalues (respectively, Flouqet multipliers for the corresponding Poincaré map) of the linearization of the system about the tori; generically, these tori are either normally elliptic[5] or normally hyperbolic[6]. If the torus has one pair of zero characteristic eigenvalues in the direction of the normal $(\overline{q}, \overline{p})$ plane, it is said to be *normally parabolic*.

---

[5]If the characteristic eigenvalues of an invariant lower dimensional torus (with respect to its normal $(\overline{q}, \overline{p})$ plane), are purely imaginary (and do not vanish), it is said to be *normally elliptic*.

[6]If all the characteristic eigenvalues of an invariant lower dimensional torus (with respect to its normal $(\overline{q}, \overline{p})$ plane) have a nonzero real part, it is said to be *normally hyperbolic*.

Locally, in the $(\overline{q}, \overline{p}, J)$ coordinate system, the normal stability of the invariant torus is determined by:

$$\det\left(\left.\frac{\partial^2 H_0}{\partial^2(\overline{q}, \overline{p})}\right|_{p_f}\right) = -\lambda_{p_f}^2 \qquad (16)$$

where p_f satisfies (15). Indeed, when λ_{p_f} is real and non-vanishing the corresponding family of tori is said to be normally hyperbolic, when it vanishes it is called normally parabolic and when it is pure imaginary it is normally elliptic, see the detailed references in [27] and the discussion of the Hamiltonian case in [9]. For our example such calculation shows that the first and third families of invariant circles become parabolic at $I = \frac{1}{2}k^2$ whereas the second and fourth families are parabolic at $I = 2k^2$:

Jacobian Eigenvalues	Elliptic For	Hyperbolic For	Parabolic For
1. $(\lambda_{pw})^2 = k^2(-k^2 + 2I)$	$I < \frac{1}{2}k^2$	$I > \frac{1}{2}k^2$	$I_p^{pw} = \frac{1}{2}k^2$
2. $(\lambda_{sm})^2 = \left(\frac{3}{2}I + k^2\right)\left(\frac{1}{2}I - k^2\right)$	$I < 2k^2$	$I > 2k^2$	$I_p^{sm} = 2k^2$
3. $(\lambda_{pwm})^2 = \frac{4}{7}(2k^4 - k^2I - 6I^2)$	$I > \frac{1}{2}k^2$	-	$I_p^{pw} = \frac{1}{2}k^2$
4. $(\lambda_{smm})^2 = 4k^2(2k^2 - I)$	$I > 2k^2$	-	$I_p^{sm} = 2k^2$

Table 2

3.1 Energy momentum bifurcation diagrams and the branched surfaces

The *energy-momentum bifurcation diagram (EMBD)* supplies global information on the bifurcations of the energy surfaces structure and their relation to resonances; Consider an integrable Hamiltonian system $H_0(q, p)$ in a region $D \subseteq M$ at which a transformation to the local generalized coordinate system $H_0(\overline{q}, \overline{p}, J)$ is non singular. The energy-momentum map assigns to each point of the phase space $(\overline{q}, \overline{p}, J)$ a point in the energy-momentum space $(h = H_0(\overline{q}, \overline{p}, J), J)$. The Energy-Momentum bifurcation diagram (EMBD) is a plot in the (h, J) space (for (h, J) in the range of D) which includes:

- The region(s) of allowed motion (the closure of all regions in which the energy-momentum mapping is a trivial fibre bundle, see [1], [35]).

- The singular surfaces $(h, J) = (H_0(p_f), J_f)$ (see equation (15)) where the normal stability of the corresponding singular $(n-1)$-tori, defined by equation (16), is indicated.

- The strongest resonance surfaces on which the inner frequencies of the tori vanish, $\omega_i = 0$ (and possibly the regions in which back-flow occurs, where $\frac{d\phi_i(\bar{q},\bar{p},J)}{dt}$ changes sign along the level set $(h = H_0(\bar{q}, \bar{p}, J), J)$ for some $i = 1, ..., n-1$).

- The energies at which topological bifurcations occur and the branched surfaces (Fomenko graphs if $n = 2$) in the intervals separated by these bifurcation points.

The energy-momentum bifurcation diagram depends on the choice of the generalized action-angle co-ordinates $(\bar{q}, \bar{p}, J)$, see [27] for discussion. In particular, *the form of the perturbation* determines what are the strongest resonant directions, and the actions in the EMBD are chosen accordingly. Here, eq. (9) implies that the dominant resonant direction is indeed the conjugate angle to I, in both the (x, y, I) and the (u, v, I) co-ordinate systems. Hence, the convenient coordinates for the energy-momentum bifurcation diagram is (h, I). Notice that while the momentum variable I is globally defined, the associated angle co-ordinate is defined differently near the plane wave circles $(b = 0)$ and near the symmetric mode circles $(c = 0)$. The EMBD contains the resonance information for both representations.

3.2 Construction of the EMBD

Calculation of the singular surfaces and the normal stability of the lower dimensional tori are the first steps in depicting the global structure of the energy surfaces. We begin the construction of the EMBD by plotting the singular surfaces $(H_0(p_f(I)), I)$ in the (h, I) plane, where $(p_f(I))$ are given by the six families of Table 1:

$H_0(x_f, y_f, I)$ Evaluation	Exist For
1. $H(x_{pw}, y_{pw}, I) = H(0, 0, I) = (\frac{I^2}{2} - I)$	$I \geq 0$
2. $H(u_{sm}, v_{sm}, I) = H(0, 0, I) = \frac{3}{4}I^2 - Ik^2 - I$	$I \geq 0$
3. $H(x_{pwm}^{\pm}, y_{pwm}^{\pm}, I) = \frac{15}{14}I^2 - (1 + \frac{4}{7}k^2)I + \frac{1}{7}k^4$	$I \geq \frac{1}{2}k^2$
4. $H(u_{smm}^{\pm}, v_{smm}^{\pm}, I) = \frac{I^2}{2} - I - k^4$	$I \geq 2k^2$

Table 3

In figure 1 we plot these curves for the non-dimensional wave number $k = 1.025$, which is the value used in previous works [4, 2, 8, 5, 3, 6]. Other values of k are presented in Appendix B. We use the usual convention in bifurcation diagrams by which normally stable circles are denoted by solid lines whereas normally hyperbolic circles are denoted by dashed lines (see Table 2). Different colors are used for the different families of invariant circles (Thick and thin black line[7] for the plane wave and its bifurcating branch and thick and thin grey line[8] for the symmetric mode and its bifurcation branch). The allowed region of motion is shaded - for each point (h, I) in this shaded region there are (c, b) values satisfying $H_0(c, b) = h, I = \frac{1}{2}(|c|^2 + |b|^2)$. An energy surface in this diagram is represented by the intersection of a vertical line with the allowed region of motion. The topology of the level sets for different I values on a given energy surface is represented by the Fomenko graphs as described next.
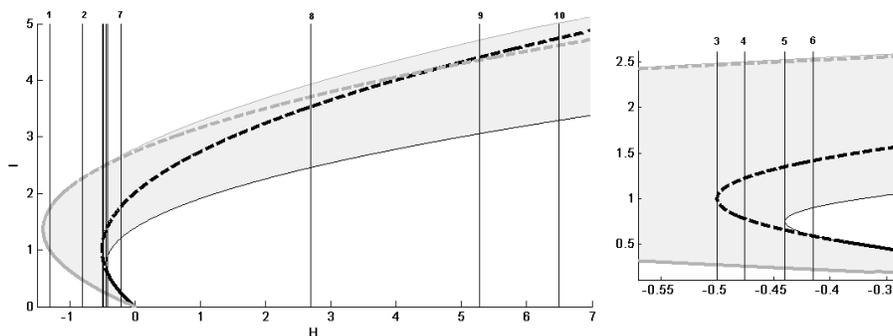

Figure 1. EMBD graph for $k = 1.025$. Thick black line- p_{pw}, Thin black line - p_{pwm} Thick grey line- p_{sm}, Thin grey line - p_{smm}

3.3 Fomenko graphs.

The Fomenko graphs are constructed by assigning to each connected component of the level sets (on the given energy surface) a point on the graph, so there is a one-to-one correspondence between them. In this way the topological changes of the level sets are discovered and the energy surface may be reconstructed from these graphs.

---

[7]blue and red
[8]magenta and green
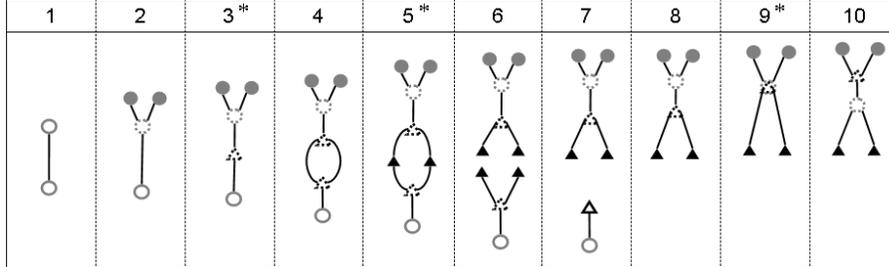
Figure 2. Fomenko graphs for $k = 1.025$.

Consider for example figures 1, 2 and 3; Figure 1 is the energy-momentum bifurcation diagram for the truncated NLS model at $k = 1.025$. The numbered vertical lines on this figure indicate energy values for which the Fomenko graphs where constructed as shown in figure 2. Finally, the third figure shows the energy surface (modulus the angle circle) at the energy level corresponding to line 5 in figure 1 and to diagram 5 in figure 2. The energy surface is plotted twice; it is the two dimensional surface in the (x, y, I) space (respectively (u, v, I) space) multiplied, for all $c \neq 0$ (for all $b \neq 0$), by the circle $\gamma \in S^1$ ($\theta \in S^1$). The redundant presentation in the (u, v, I) space is shown to better explain the level sets topology near the circle $c = 0$ where the transformation to the (x, y, I) co-ordinates is singular.

On the Fomenko graphs, we denote the invariant circles corresponding to the plane wave family (p_{pw}) and the invariant circles which emanate from them ($p_{pwm}^{\pm}$), by open and full triangles respectively (for clarity, the boundary of the triangle is dashed when it is normally hyperbolic and full when it is normally elliptic). The invariant circles corresponding to the symmetric mode family (p_{sm}) and the invariant circles which emanate from them ($p_{smm}^{\pm}$), are denoted by open and full circles, again with the usual convention for the stability.

Let us describe in details the level sets topology on this energy surface as the action I is increased. The lowest I value corresponds to the intersection of line 5 with the solid grey line in figure 1, to the open circle on the Fomenko graph and to the lowest level set in figure 3 - the symmetric mode circle. The level set here is the circle $c = 0, |b| = \sqrt{2I_{sm}}$ which is normally elliptic. It is represented in the (u, v) plane as a point - the origin - which is multiplied by the circle in θ (the representation in the (x, y) plane is singular here). For a bit larger I values each level set is composed of one torus - the Fomenko graph has a single edge for

such values of I and indeed we see that in both the (x, y) plane and the (u, v) plane a single circle, corresponding to a torus, appears. When the I value reaches the dashed black line in figure 1 the level set becomes singular - it is composed of the plane wave circle and its homoclinic surfaces, shown as a figure-eight level set in the (x, y) plane. On the three dimensional energy surface this figure eight is multiplied by the circle $\gamma \in S^1$. This singular level set is denoted by the open triangle with dashed boundary in the Fomenko graph. As I is increased beyond this I value, each point in the (h, I) plane has two tori associated with it - in the Fomenko graph we see that there are two edges for these values of I, and the corresponding level sets at the (x, y) plane have two disconnected circles. These circles shrink to two points which are two normally elliptic invariant circles of the plane-wave-mixed-mode type at a critical I value at which line 5 is tangent to the curve corresponding to p_{pwm} in figure 1; For energies above line 5 the energy surface splits to two due to this curve. Thus this value of the energy is an energy bifurcation value - the level sets for lower energies (diagram 4) and higher energies (diagram 6) undergo different topological changes as the action is increased along the energy surface (graphs corresponding to such energy bifurcation values are denoted here by * in the Fomenko graph sequences). The two circles $p_{pwm}^{\pm}$ are denoted by the solid triangles in the Fomenko graph. Further increase of I leads us again to the two tori situation until the curve p_{pw} is intersected again. Then the two tori coalesce at the singular level set of the plane wave and its homoclinics which is denoted as before by an open triangle. Further increase of I leaves us with one connected component of the level sets until the dashed grey line in the EMBD, which denotes the normally hyperbolic circles p_{sm}, is intersected. This singular level set is again, topologically, a figure-eight times a circle, but now it is represented in the u, v plane (since the (x, y) coordinates are singular here). It is denoted in the Fomenko grpah by an open circle from which, for larger I values, two edges emanate. These correspond to the two tori which oscillate near the two symmetric-mode-mixed-mode circles. The upper boundary of the energy surface is reached when these two tori shrink to the corresponding invariant circles - when line 5 intersected the thin grey line - when the two solid circles in the Fomenko graph are reached.

This rather lengthy explanation can be now repeated for each Fomenko graph without the explicit computation of the corresponding energy surfaces. Namely, these graphs encode all needed information for the reconstruction of the energy surfaces. We note that a similar construction for some n d.o.f. systems has been recently suggested (see [27] and references therein).
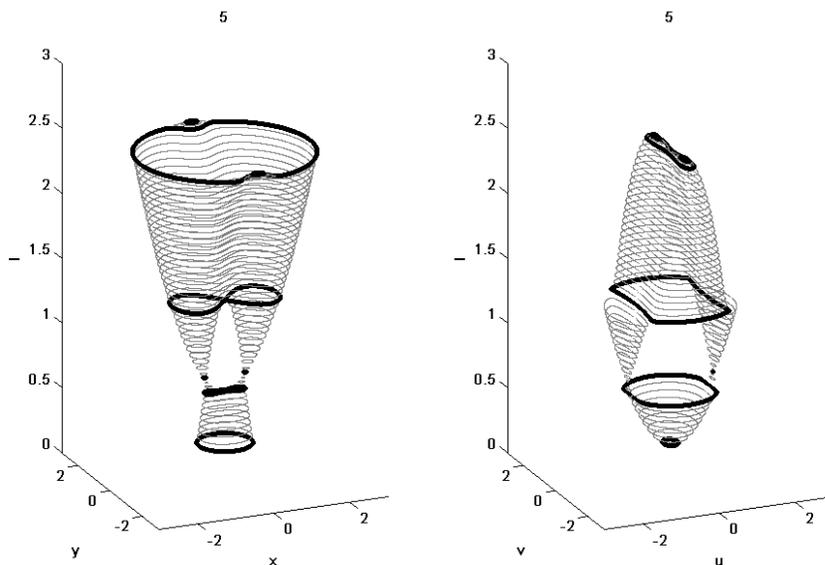
Figure 3. Corresponding energy surface for Fomenko graph 5 of figure 2. Level sets marked by black thick lines correspond to vertices in the graph.

4. Hierarchy of bifurcations

Given an integrable family of Hamiltonian systems $H_0(\overline{q}, \overline{p}, J; \mu)$ depending on the vector of parameters μ there is a hierarchy of bifurcation scenarios:

- Single energy surface. The first level consists of the values of the constants of motion across which the topology of the level sets on a given energy surface $H_0(\overline{q}, \overline{p}, J; \mu) = h$ is changed. These are the values at which the singularity surfaces cross the vertical hyperplane $H_0 = h$ on the EMBD, and correspond to the vertices in the Fomenko graphs.

- Energy bifurcation values. The second level consists of the energy bifurcation values h^b at which the form of the Fomenko graph changes, namely across which the energy surfaces are no longer equivalent. Thus, it describes how the energy surface geometry is changed with h.

- Parameter dependence of the energy bifurcation values. The third level consists of the bifurcating parameter values μ^b at which the bifurcation sequence of the second level changes (by either chang-

ing the order of the energy bifurcating values or by adding/substracting one of the energy bifurcation values).

Most previous works have concentrated on the first level alone, by which the topology of level sets on a given energy level are studied. For a large class of systems the Fomenko graphs (and the corresponding branched surfaces in higher dimensions) provide a full description of this level. Appendix B includes a few more representative cases for the truncated NLS model. The second level, which is represented by the EMBD, is discussed next.

4.1   Bifurcating Energy values.

Intersecting the energy-momentum bifurcation diagrams with a vertical line (hyper-surface in the n d.o.f. case) and constructing the corresponding Fomenko graphs (branched surfaces) leads to a full description of a given energy surface. It follows that changes in the topology of the energy surfaces can be easily read off from these diagrams - folds, branchings, intersections and asymptotes of the singularity surfaces - may all result in such changes. The dynamical phenomena associated with each of these simplest geometrical features of the singularity surfaces are listed below. We note that a complete classification of all the possible singularities of these singularity surfaces and their dynamical consequences has not been developed yet.

Folds in the singularity surfaces and Resonances.   Clearly (see for example figure 1) the energy surfaces change their topology whenever there is a fold in the singularity surfaces. Furthermore, it was established in [27] that folds of non-parabolic singularity surfaces correspond to strong resonance relations for the lower dimensional invariant tori:

$$\frac{dH}{dJ_i}(p_f^*) = 0 \Leftrightarrow \dot{\phi}_i\bigg|_{p_f^*} = 0, i = 1, ..., n - 1.$$

In particular, a fold of the singularity surface $H_0(\overline{q}_f, \overline{p}_f, J_f)$ at the non-parabolic torus $(\overline{q}_f, \overline{p}_f, J_f)$ implies that this $n - 1$ dimensional torus is $n - 1$ resonant, namely it is a torus of fixed points. The normal stability of this torus may be elliptic or hyperbolic. To find a set of bifurcating energies we need to list the extremum of the surfaces $H_0(\overline{q}_f, \overline{p}_f, J_f)$ for the various singularity manifolds and verify that these are non-degenerate. In Table 4 we list the I values for which folds are created for the six singular surfaces of Table 3. The values of I for which the singular circles are parabolic are listed as well.

$\frac{dH}{dI}(x_f, y_f, I_f) = 0$	I-resonance	I-parabolic	Parabolic Resonance
1. $(I - 1) = 0$	$I_r^{pw} = 1$	$I_p^{pw} = \frac{1}{2}k^2$	$k_{pr-pw} = \sqrt{2}$
2. $\frac{3}{2}I - k^2 - 1 = 0$	$I_r^{sm} = \frac{2k^2+2}{3}$	$I_p^{sm} = 2k^2$	$k_{pr-sm} = \sqrt{\frac{1}{2}}$
3. $\frac{15}{7}I - 1 - \frac{4}{7}k^2 = 0$	$I_r^{pwm} = \frac{4k^2+7}{15}$	$I_p^{pw} = \frac{1}{2}k^2$	$k_{pr-pw} = \sqrt{2}$
4. $(I - 1) = 0$	$I_r^{smm} = 1$	$I_p^4 = 2k^2$	$k_{pr-sm} = \sqrt{\frac{1}{2}}$

<div align="center">Table 4</div>

Using the resonant I values of Table 4 in Table 3 we conclude that the following energy values correspond to bifurcations due to the resonances/folds:

$$
\begin{aligned}
h_r^{pw} &= -\frac{1}{2}, \\
h_r^{sm} &= -\frac{1}{3}k^4 - \frac{2}{3}k^2 - \frac{1}{3}, \\
h_r^{pwm} &= \frac{1}{15}k^4 - \frac{4}{15}k^2 - \frac{7}{30}, \quad \text{for } k < \sqrt{2} \\
h_r^{smm} &= -\frac{1}{2} - k^4, \qquad \text{for } k < \frac{1}{\sqrt{2}}
\end{aligned}
\tag{17}
$$

At each of these energies the corresponding family of circles (for example p_{pw}) has a circle of fixed points (the open triangle in diagram 3 * in figure 2, which corresponds to a normally hyperbolic circle of fixed points giving rise to hyperbolic resonance under perturbations); for energies below the bifurcating energy (say for $h < h_r^{pw}$, see diagrams 1 and 2 there) the energy surfaces do not include any circle of this family whereas for energies beyond this value (say for $h > h_r^{pw}$, diagram 4-10 there) two circles of this family appear on the same energy surface.

Branching surfaces and parabolic circles. Another source for bifurcations in the energy surface structure appears when the singularity surface splits. For the two degree of freedom case such a splitting is associated with the appearance of a parabolic circle (for the n d.o.f. case we look for a fold in the surface of parabolic tori, namely we look for an $n-2$ resonant parabolic $n-1$ tori, see [27] for precise statement). Thus, the appearance of the parabolic circle p_{sm} at $h = h_p^{sm}$ from which the branches of circles $p_{smm}^{\pm}$ emerge implies that for energies below this value (graph 1 in figure 2) no such circles appear, and the Fomenko graph

has no splitting to two branches whereas larger energies have these two circles as the upper boundary of the energy surface (diagrams 2-10). In Table 4 we list the parabolic values of I. Plugging these values in Table 3 we find two additional values of energy bifurcations which appear due to singularity surface branchings:

$$h_p^{pw} = \frac{1}{2}k^2(\frac{1}{4}k^2 - 1), \quad h_p^{sm} = k^4 - 2k^2 \tag{18}$$

Singular surfaces crossings and Global bifurcation.   A third possible source for topological changes in the energy surface is the crossing of singular surfaces. Such an intersection of singular surfaces of $n-1$ dimensional invariant tori can be a result of one of the following phenomena:

1 Appearance of a higher dimensional singularity, namely an $n-2$ invariant torus.

2 Appearance of a global bifurcation - e.g. the creation of heteroclinic connection between two families of $n-1$ normally hyperbolic families.

3 Appearance of two disconnected and unrelated singular level sets for the same action and energy values.

Each one of these phenomenon appears to be persistent under C^r integrable perturbation with $r > 2$. The first and second cases imply that the corresponding energy is a bifurcating energy value, whereas the third does not. For our example, it follows from Table 3 that the two curves $(H(p_{pw}(I)), I)$ and $(H(p_{sm}(I)), I)$ cross at $I = 0$ and at $I = I_{gb} = 4k^2$ and that no other singularity curves cross.

$I = 0$ corresponds to the trivial solution $c = b = 0$, at which both singularity curves are normally elliptic and at their intersection we have a $4d$ elliptic point - an $n-2$ singular level set, as in the first case above. Thus the corresponding energy, $h_0 = 0$, is an energy bifurcation value.

$I_{gb} = 4k^2$ corresponds to the intersection of the two singularity curves (of p_{pw} and p_{sm}) at a value for which both families are normally hyperbolic (since $I_{gb} > I_p^{sm} = 2k^2 > I_p^{pw} = \frac{1}{2}k^2$ for all $k > 0$, see Table 2). Indeed, at this value our system admits four heteroclinic connections between the plane wave circles and the symmetric mode circles (see [22]). The energy-momentum bifurcation diagrams (see figure 1) show the intersection between the corresponding singularity curves (dashed grey and dashed black). The Fomenko graphs (graphs 8,9,10 in figure 2) demonstrate that a global bifurcation must occur - the solid circles (denoting $p_{smm}^{\pm}$) are connected to the open circle (denoting p_{sm} and its

homoclinic orbits) in graph 8 and to the open triangle (denoting p_{pw} and its homoclinic orbits) in graph 10. Hence, this intersection corresponds to a global bifurcation and the corresponding energy is an energy bifurcation value. Summarizing, we find two additional energy bifurcation values which appear from singularity surfaces crossings:

$$h_0 = 0, \quad h_{gb} = 4k^2(2k^2 - 1) \tag{19}$$

Unbounded singularity surfaces. Another possible source for an energy bifurcation value is the appearance of a critical energy at which one of the singularity surfaces tends to infinity (i.e. $(H_0(p_f), J_1, .., J_{n-1}) \rightarrow (h_c, J_1^c, ..., J_{j-1}^c, \infty, J_{j+1}^c, ..J_{n-1}^c)$, with possibly more than one infinite direction, see [35]). In this case energy surfaces become unbounded in the J_j direction after this critical energy value. This possibility does not appear in our model and may be associated with the existence of unbounded level sets.

4.2 Bifurcation diagram of the EMBD.

We are now ready to describe the third level of the bifurcation hierarchy - the dependence of the EMBD's on the parameter of the problem, the wave number k. Equations (17,18,19) include the eight energy bifurcation values for our model. At these values of energies the energy surface structure changes. Hence, the order of these bifurcation values determines the sequence of changes of the energy surface topology. In particular, at k values for which pairs of these curves cross, degenerate bifurcation occur, and the bifurcation sequence of the Fomenko graphs changes. Figure 4 shows the graph of the eight curves $h_r^{pw}, h_p^{pw}, h_r^{sm}, h_p^{sm}, h_r^{pwm}, h_r^{smm}, h_{gb}, h_0$ as a function of k. This is a bifurcation diagram of the energy bifurcation values - *crossings of curves in this diagram correspond to bifurcations of the EMBD's.* The emerging picture is complicated - there are 13 intersections of these curves, so a complete description of the truncated NLS model consists of 14 different EMBD figures and their corresponding Fomenko graph sequences. A few representative ones are shown in Appendix B. Let us discuss the dynamical consequences of a few of these crossings.

Parabolic Resonances. When the curve corresponding to a fold (circle of fixed points), and the curve corresponding to the parabolic circles intersect, a parabolic circle of fixed points is created. Indeed, at the critical value $k = k_{pr-pw} = \sqrt{2}$ (respectively at $k = k_{pr-sm} = \frac{1}{\sqrt{2}}$) the plane wave family, $b = 0$, (respectively the symmetric mode family, $c = 0$) possesses a parabolic resonant circle at $I_{pr} = 1$; at this value of the
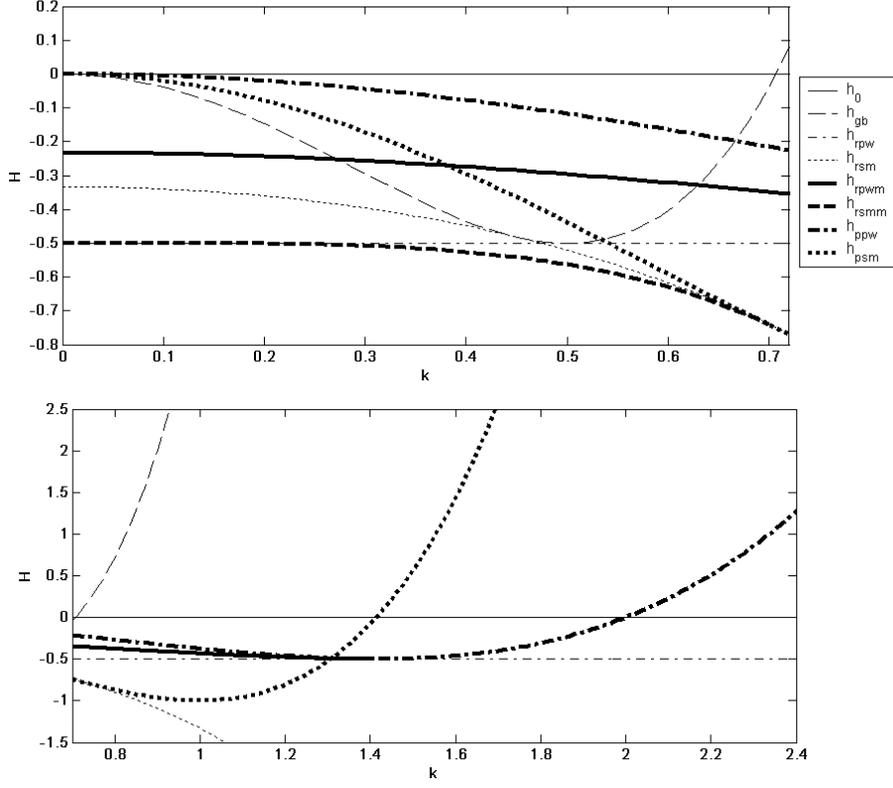
Figure 4. Bifurcation diagram of the energy bifurcation values.

parameter three bifurcating energy curves intersect $h_r^{pw} = h_p^{pw} = h_r^{pwm}$ (similarly, at $k = k_{pr-sm}$, $h_r^{sm} = h_p^{sm} = h_r^{smm}$), see figure 4. The corresponding EMBD has therefor a fold occurring exactly at the point at which the singularity curve changes from solid to a dashed line.

The appearance of parabolic resonances gives rise to trajectories which have different characteristics than trajectories appearing in 1.5 d.o.f. systems as shown below for our model. In general, it is observed (see [34]) that large instabilities occur near parabolic resonances when additional degeneracies occur - when the curvature of one of the branches at the parabolic resonant points approaches zero and a near flat PR appears (see [26, 25] for the higher dimensional formulation and examples):

$$\frac{d^2}{dJ^2} H_0(x(J), y(J), J) \bigg|_{p_f \to p_f^{pr}} \to 0.$$

Here, we find that $\left.\frac{d^2}{dI^2}H_0(x(I),y(I),I)\right|_{\{p_{pw},p_{sm},p^\pm_{pwm},p^\pm_{smm}\}} = \{1,\frac{3}{2},\frac{15}{7},1\}$, namely these are fixed non-vanishing numbers. Hence, we conclude that the instability mechanism associated with the near-flat resonance does not exist in this model. It follows that an introduction of additional parameter which controls, for example, the mixed terms in the Hamiltonian $H_0(x,y,I)$ can alter this property and induce strong instabilities.
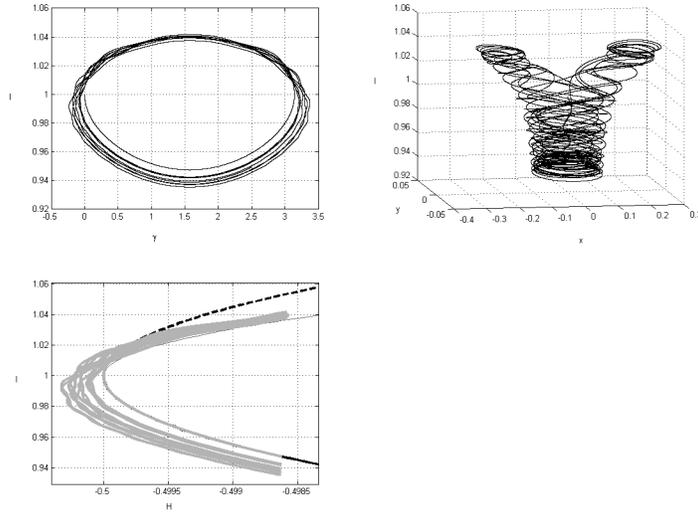

Figure 5. Parabolic resonance near $b = 0$ with $H_1 \propto c - c^*$, $k = \sqrt{2}$

We present simulations showing the instabilities near the two parabolic resonant circles at $k = \sqrt{2}$ and $k = 1/\sqrt{2}$ respectively. The instabilities are similar to those observed for other PR systems, in the regime which is non-degenerate. Notice that near the symmetric mode circle the perturbation term is small since the perturbed Hamiltonian is proportional to c. In figures 6 and 8 we add a perturbation which is proportional to b, and then one observes a much more pronounced instability. Such a perturbation corresponds to adding a first Harmonic term to the perturbation term, namely adding to the Sine-Gordon equation a perturbation of the form $\varepsilon\Gamma_1\cos(\frac{2\pi n}{L}x)\cos(\omega t)$ which corresponds to considering in the truncated two mode Hamiltonian model the perturbation:

$$H_2(c,c^*,b,b^*) = -\frac{i}{\sqrt{2}}(c-c^*) - \frac{\Gamma_1 i}{\sqrt{2}}(b-b^*). \qquad (20)$$

In the figures we use the appropriate co-ordinate system for each case - the (x,y,I,γ) system near the $b = 0$ circle (figures 5 and 6 and the
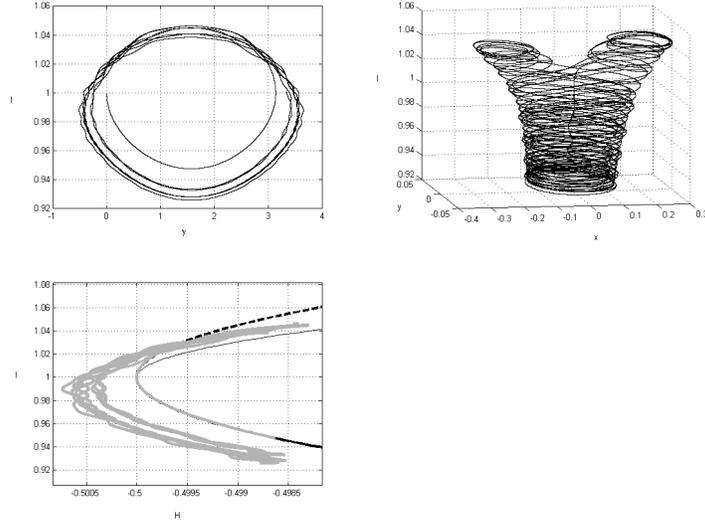
Figure 6. Parabolic resonance near $b = 0$ with $H_1 \propto (c - c^*) + (b - b^*)$, $k = \sqrt{2}$

(u, v, I, θ) system near the $c = 0$ circle. The projections of the trajectory on the energy-momentum bifurcation diagram are shown as well - these demonstrate that the singularity surfaces dominate the perturbed motion.
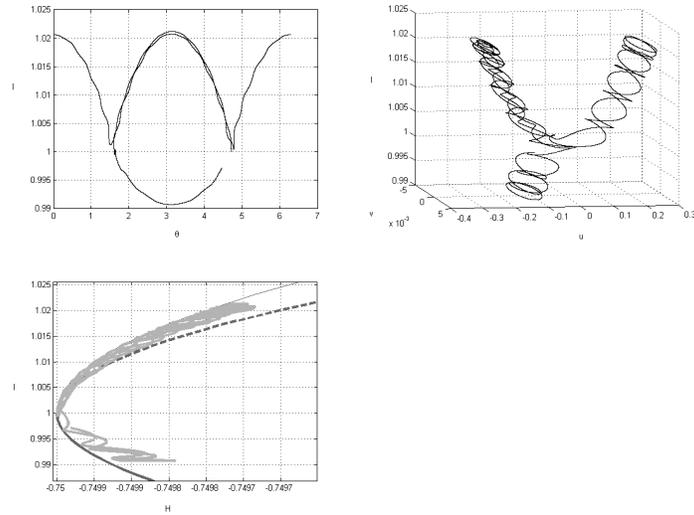

Figure 7. Parabolic resonance near $c = 0$ with $H_1 \propto (c - c^*)$, $k = 1/\sqrt{2}$
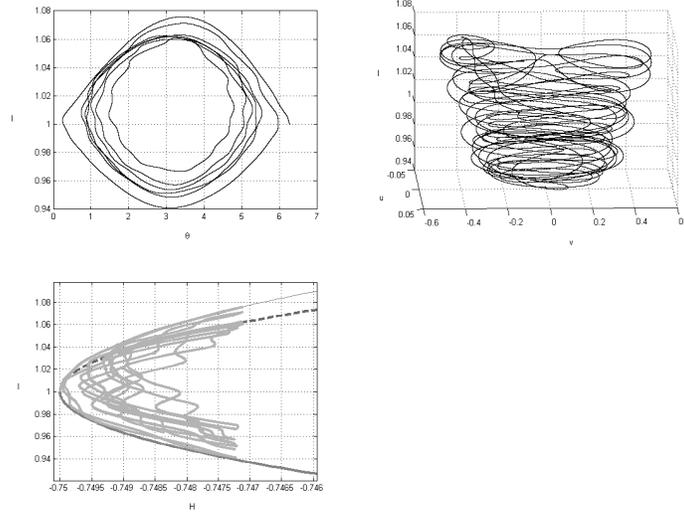
Figure 8. Parabolic resonance near $c = 0$ with $H_1 \propto (c - c^*) + (b - b^*)$, $k = 1/\sqrt{2}$

Resonant global bifurcation. When the global bifurcation curve and the curve corresponding to a fold (circle of fixed points) intersect, a heteroclinic connection between an invariant hyperbolic circle of fixed points and an invariant hyperbolic circle is created. Such intersections occur when: $h_{gb} = h_r^{pw}$ and when $h_{gb} = h_r^{sm}$. Simple calculation shows that these scenarios occur at $k = \frac{1}{2}$ and $k = \frac{1}{\sqrt{5}}$ respectively:

$$I_r^{pw} = 1 = I_{gb} = 4k^2 \Leftrightarrow k = \frac{1}{2}$$

$$I_r^{sm} = \frac{2k^2 + 2}{3} = I_{gb} = 4k^2 \Leftrightarrow k = \frac{1}{\sqrt{5}} = .4472...$$

In fact, as is seen from figure 4, and may be easily verified at $k = \frac{1}{2}$ (respectively at $k = \frac{1}{\sqrt{5}}$) the curves h_{gb} and h_r^{pw} (respectively h_r^{sm}) are tangent. It implies that for k values in the range $(.4472, .5)$ near resonant behavior of both circles involved in the global bifurcations are expected if ϵ is not too small.

Geometrically, at these values of k the unperturbed system has a circle of fixed points (at $p_{pw}(I_{rgb-pw})$ and $p_{sm}(I_{rgb-sm})$ respectively, see Table 5) which has four families of heteroclinic connections to a periodic orbit (at $p_{sm}(I_{rgb-pw})$ and $p_{pw}(I_{rgb-sm})$ respectively). The behavior of such a structure under small perturbations has not been analyzed yet to the best of our knowledge. Simulations near these two values reveal

an intriguing picture of instability which are not well understood yet. Below a representative simulation is presented.
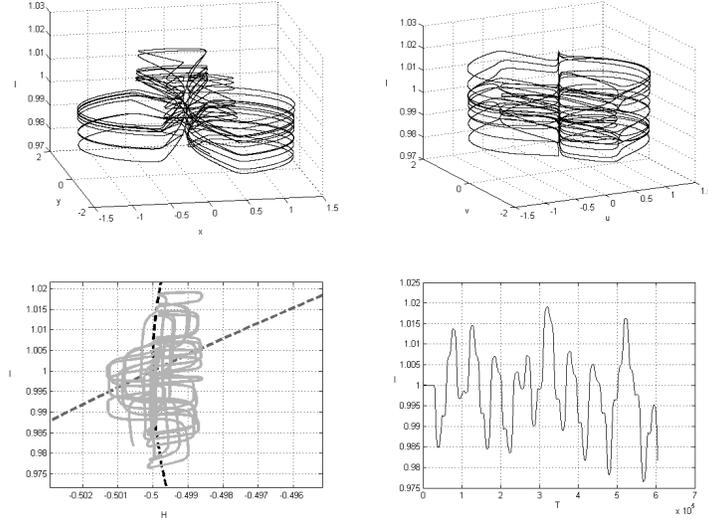

Figure 9. Global resonant bifurcation - $k = \frac{1}{2}$

Other crossings. Notice that several other crossings exist - these do imply topological changes on the sequences of the Fomenko graphs but do not imply that the local qualitative behavior of solutions will be altered. For example, the global bifurcation energy and the parabolic bifurcation energy of the two corresponding circles cross when $h_{gb} = h_p^{pw}$ and when $h_{gb} = h_p^{sm}$. However, it is immediately seen that the I values at which the global bifurcations occurs ($I_{gb} = 4k^2$) and the I values at which parabolicity appears ($I_p^{pw} = \frac{1}{2}k^2, I_p^{sm} = 2k^2$) are well separated for all k values which are bounded away from 0. Hence the dynamics associated with these two phenomena appear on separate phase space regions and the coincidence of these two energy bifurcation values is not dynamically significant.

Finally, at $k = 0$ many of the energy bifurcation curves cross. Indeed, in the limit of small k we expect quite a complicated behavior as many of the bifurcations occur for very close by I values and the curvature of all the curves in the EMBD are quite small. As we have mentioned - small curvature means degeneracies and strongest possible instabilities. However, it appears that here all these phenomena are associated with small I values.

5.   Conclusions.

The analysis of the truncated model introduced by Bishop et al. two decades ago revealed two types of instabilities which have not been previously observed nor analyzed in this context - the parabolic resonance and the global resonance circles. It is still unknown whether and how these scenarios will appear in the PDE model - hopefully these will turn out to produce infinite dimensional analogs as did the hyperbolic resonance scenario.

While investigating this particular model we have realized that a complete bifurcation analysis of a family of near integrable Hamiltonian system involves a hierarchy of three levels - the bifurcation of level sets on a given energy surface, the bifurcation of the energy surfaces structure which may occur via several mechanisms (resonances, global bifurcations, resonant parabolic circles and the appearance of unbounded energy surfaces) and finally the bifurcating energies dependence on the parameters. The list of bifurcation values at each level may be quite long. It appears that some are more dynamically significant than others, yet a quantifier for such qualitative observations is still lacking. The appearance of global bifurcations as a persistent phenomenon in higher dimensional system is another intriguing direction of research which we hope to develop in the future.

Acknowledgment

Appendix: A

It is proved that the perturbed energy surfaces of the truncated NLS model are bounded and that they are close to the unperturbed surfaces. First, notice that the unperturbed energy surfaces are bounded in c, b since all the quartic terms have positive coefficients:

$$H_0 = \frac{1}{8}|c|^4 + \frac{3}{16}|b|^4 + \frac{1}{2}|b|^2|c|^2(1 + \frac{1}{2}\cos(2\arg(bc^*))) - \frac{1}{2}(1+k^2)|b|^2 - \frac{1}{2}|c|^2 \quad \text{(A.1)}$$

Since $H = H_0 + \varepsilon O(|c|, |b|)$ it follows immediately that the perturbed surfaces are bounded as well. Denote by $c_{\max}^{h,\varepsilon}$, $b_{\max}^{h,\varepsilon}$ the maximal amplitude of c, b on the energy surface $H(c, c^*, b, b^*; \varepsilon) = h$:

$$c_{\max}^{h,\varepsilon} = \max\{|c| : H(c, c^*, b, b^*; \varepsilon) = h\}$$
$$b_{\max}^{h,\varepsilon} = \max\{|b| : H(c, c^*, b, b^*; \varepsilon) = h\}$$

it follows from (A.1) that for $h \gg 1$, $c_{\max}^{h,0}, b_{\max}^{h,0} = O(\sqrt[4]{h})$. Furthermore, it can be shown, using the form of eq. (6), that for large values of h the system cannot have fixed points. In fact, one can prove the following:

Lemma. There exists an $h^*(k)$ such that for all $h > h^*(k)$ $\left\|\nabla H_0|_{H_0(c,c^*,b,b^*)=h}\right\| \neq 0$.

Proof. Let us find all solutions to $\left\|\nabla H_0|_{H_0(c,c^*,b,b^*)=h}\right\| = 0$. Clearly at $c = b = 0$ $\nabla H_0|_{H_0(c,c^*,b,b^*)=h}$ so $h^*(k) > 0 = H_0(0,0,0,0)$. Using the non-singular transformation to the (x, y, I, γ) co-ordinates for $c \neq 0$, and the non-singular transformation to the (u, v, I, θ) co-ordinates when $b \neq 0$, it follows that $\left\|\nabla H_0|_{H_0(c,c^*,b,b^*)=h}\right\| = 0$ only when the invariant circles of table 1 are circles of fixed points, namely at the resonant I values, $I = I_r$, of table 4. Plugging these resonant I values in table 3, we find that circles of fixed points appear at the following h values: $H_0(p_{f-res}) = \{-\frac{1}{2}, -\frac{1}{3}k^4 - \frac{2}{3}k^2 - \frac{1}{3}, \frac{1}{15}k^4 - \frac{4}{15}k^2 - \frac{7}{30}, -\frac{1}{2} - k^4\}$. It follows that for all $h > \frac{1}{15}k^4$ there are no fixed points on the energy surfaces. $\square$

In fact, it follows from (6) that for h sufficiently large, *for all* (c, b) satisfying $H_0(c, c^*, b, b^*) = h$ we have:

$$\max\{\left|\frac{\partial H_0(c, c^*, b, b^*)}{\partial b^*}\right|, \left|\frac{\partial H_0(c, c^*, b, b^*)}{\partial c^*}\right|\} \geq Ch^{3/4}.$$

It follows from the implicit function theorem and the form of the perturbation (namely since H_i $(i = 1, 2)$ are linear in c, b so that $|H_i| < O(\sqrt[4]{h})$), that for $\varepsilon = o(\sqrt{h})$

$$c_{\max}^{h,\varepsilon} = c_{\max}^{h,0} + O(\frac{\varepsilon}{\sqrt{h}})$$
$$b_{\max}^{h,\varepsilon} = b_{\max}^{h,0} + O(\frac{\varepsilon}{\sqrt{h}})$$

Similarly, by the implicit function theorem, when $\|\nabla H_0\| > const$, the solution to the equation

$$H(c^\varepsilon(h^\varepsilon), c^{\varepsilon*}(h^\varepsilon), b^\varepsilon(h^\varepsilon), b^{\varepsilon*}(h^\varepsilon); \varepsilon) = h^\varepsilon = h + O(\varepsilon)$$

is $\varepsilon-$close to the solution to this equation with the $\varepsilon = 0$ values. Near the fixed points the perturbed surface is expected to be $O(\varepsilon^{1/\alpha})$ close to the unperturbed one, where α is the order of the tangency of the singularity curve at the resonance.

Note that formally the larger the h the larger is the extent of the energy surface and the larger is the range of unperturbed energy surfaces which we need to consider. However, if h is very large the structure of H_0 remains asymptotically unchanged and one can verify that in fact this limit may be studied by rescaling; substituting

$$\overline{c} = \frac{c}{\sqrt[4]{h}}, \overline{b} = \frac{b}{\sqrt[4]{h}}$$

leads to:

$$H_0(c, c^*, b, b^*) = h\left(H_0(\overline{c}, \overline{c}^*, \overline{b}, \overline{b}^*) + O\left(\frac{1}{\sqrt{h}}\right) + \frac{\varepsilon}{h^{3/4}}H_i(\overline{c}, \overline{c}^*, \overline{b}, \overline{b}^*)\right)$$

namely to the near-integrable motion with finite h.

Appendix: B

A few representative EMBD and Fomenko graphs are presented. In the EMBD the thick (thin) black line corresponds to the plane wave family p_{pw} (the mixed mode emanating from it, p_{pwm}). The thick (thin) grey line corresponds to the symmetric mode family p_{sm} (the mixed mode emanating from it, p_{smm}). These curves are dashed (full) when the corresponding circle is hyperbolic (elliptic). On the Fomenko graphs, we denote the invariant circles corresponding to the plane wave family (p_{pw}) and the invariant circles which emanate from them ($p_{pwm}^{\pm}$), by open and full black triangles respectively (for clarity, the boundary of the triangle is dashed when it is normally hyperbolic and full when it is normally elliptic). The invariant circles corresponding to the symmetric mode family (p_{sm}) and the invariant circles which emanate from them ($p_{smm}^{\pm}$), are denoted by open and full grey circles, again with the usual convention for the stability.
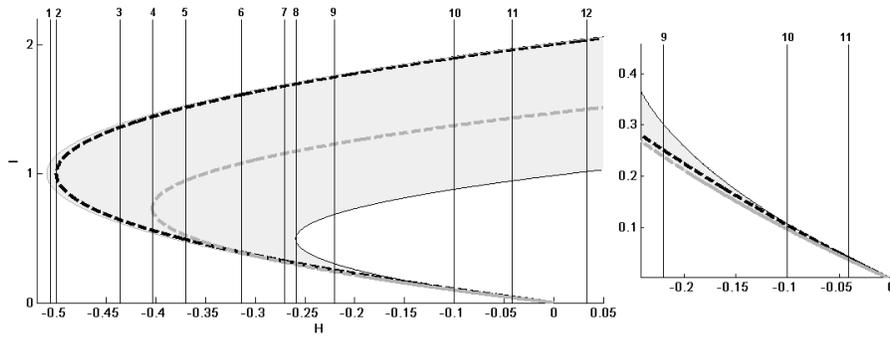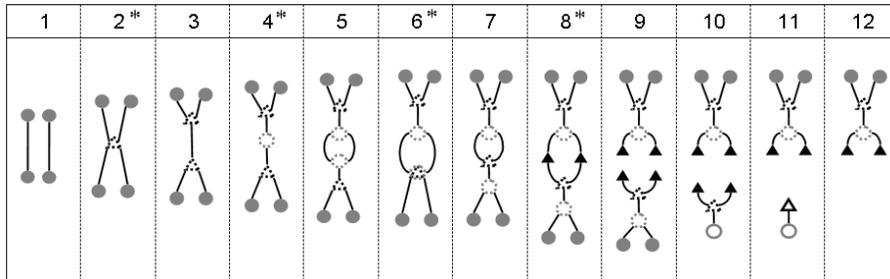

Figure B.1.   EMBD graph for $k = \sqrt{\frac{1}{10}}$.

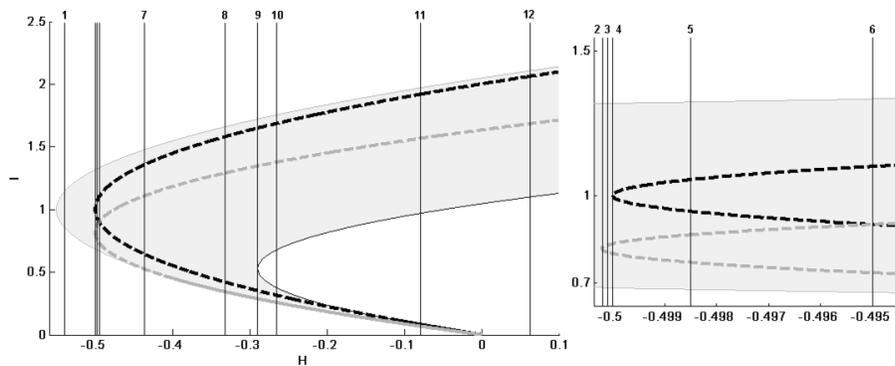Figure B.2.   Fomenko graphs figure for $k = \sqrt{\frac{1}{10}}$.
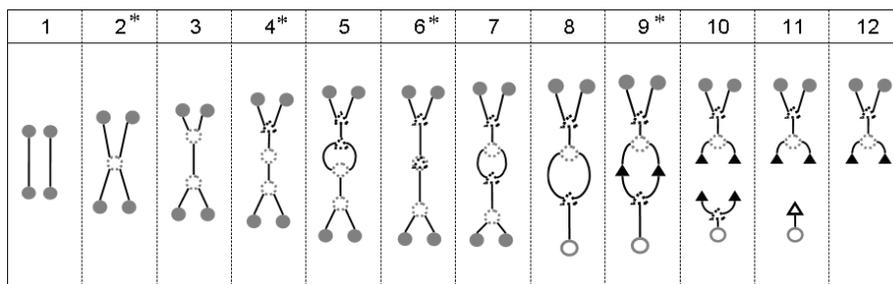
Figure B.3. EMBD graph for $k = \sqrt{\frac{9}{40}}$.

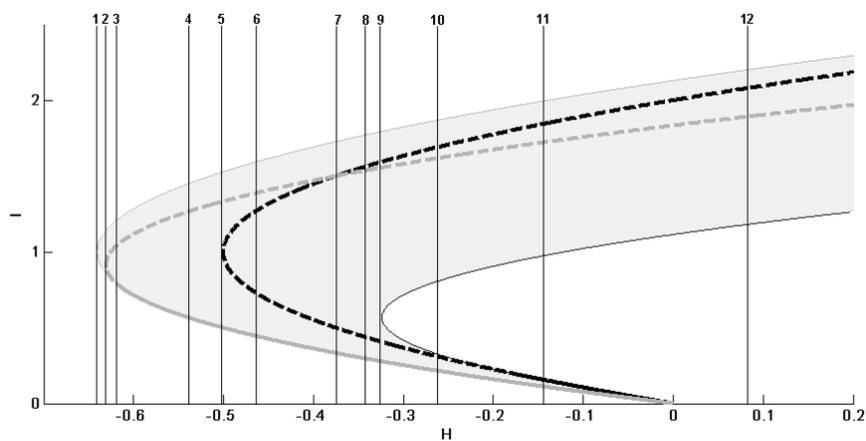*Figure B.4.* Fomenko graphs figure $k = \sqrt{\frac{9}{40}}$.

Figure B.5. EMBD graph for $k = \sqrt{\frac{3}{8}}$.

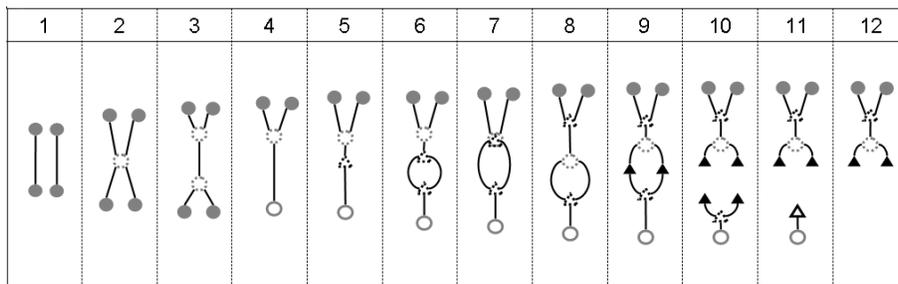*Figure B.6.* Fomenko graphs figure for $k = \sqrt{\frac{3}{8}}$.

References

[1] V. I. Arnol'd. *Dynamical Systems III*, volume 3 of *Encyclopedia of Mathematical Sciences*. Springer-Verlag, second edition, 1993.

[2] A. Bishop, R. Flesch, M. Forest, D. McLaughlin, and E. Overman II. Correlations between chaos in a perturbed sine-gordon equation and a trunctaed model system. *SIAM J. Math. Anal.*, 21(6):1511–1536, 1990.

[3] A. Bishop, M. Forest, D. McLaughlin, and E. Overman II. A quasi-periodic route to chaos in a near-integrable pde. *Physica D*, 23:293–328, 1986.

[4] A. Bishop, M. Forest, D. McLaughlin, and E. Overman II. A modal representation of chaotic attractors for the driven, damped pendulum chain. *Physics Letters A*, 144(1):17–25, 1990.

[5] A. Bishop, D. McLaughlin, M. Forest, and E. I. Overman. Quasi-periodic route to chaos in a near-integrable pde: Homoclinic crossings. *Phys. Lett. A*, 127:335–340, 1988.

[6] A. R. Bishop, K. Fesser, P. S. Lomdahl, W. C. Kerr, M. B. Williams, and S. E. Trullinger. Coherent spatial structure versus time chaos in a perturbed sine-Gordon system. *Phys. Rev. Lett.*, 50(15):1095–1098, 1983.

[7] A. R. Bishop and P. S. Lomdahl. Nonlinear dynamics in driven, damped sine-Gordon systems. *Phys. D*, 18(1-3):54–66, 1986. Solitons and coherent structures (Santa Barbara, Calif., 1985).

[8] S. Bishop and M. Clifford. The use of manifold tangencies to predict orbits, bifurcations and estimate escape in driven systems. *CHAOS SOLITONS & FRACTALS*, 7(10):1537–1553, 1996.

[9] S. V. Bolotin and D. V. Treschev. Remarks on the definition of hyperbolic tori of Hamiltonian systems. *Regul. Chaotic Dyn.*, 5(4):401–412, 2000.

[10] H. W. Broer, G. B. Huitema, and M. B. Sevryuk. *Quasi-periodic tori in families of dynamical systems: order amidst chaos*, volume 1645 of *LNM 1645*. Springer Verlag, 1996.

[11] D. Cai, D. W. McLaughlin, and K. T. R. McLaughlin. The nonlinear Schrödinger equation as both a PDE and a dynamical system. In *Handbook of dynamical systems, Vol. 2*, pages 599–675. North-Holland, Amsterdam, 2002.

[12] R. H. Cushman and L. M. Bates. *Global Aspects of Classical Integrable Systems*. Birkhauser Verlag AG, 1997.

34

[13] A. T. Fomenko. *Integrability and nonintegrability in geometry and mechanics*, volume 31 of *Mathematics and its Applications (Soviet Series)*. Kluwer Academic Publishers Group, Dordrecht, 1988. Translated from the Russian by M. V. Tsaplina.

[14] A. T. Fomenko, editor. *Topological classification of integrable systems*, volume 6 of *Advances in Soviet Mathematics*. American Mathematical Society, Providence, RI, 1991. Translated from the Russian.

[15] A. Giorgilli, A. Delshams, E. Fontich, L. Galgani, and C. Simó. Effective stability for Hamiltonian systems near an elliptic point, with an application to the restricted three body problem. *J. Diff. Eq.*, 77(1):167, 1989.

[16] G.Kovacic. Singular perturbation theory for homoclinic orbits in a class of near-integrable dissipative systems. *J. Dynamics Diff. Eqns. 5*, pages 559–597, 1993.

[17] G. Haller. *Chaos Near Resonance*. Applied Mathematical Sciences; 138. Springer-Verlag, NY, 1999.

[18] G. Haller and S. Wiggins. Multi-pulse jumping orbits and homoclinic trees in a modal truncation of the damped-forced nonlinear schrödinger equation. *Physica D*, 85(3):311–347, 1995.

[19] G. Haller and S. Wiggins. N-pulse homoclinic orbits in perturbations of resonant Hamiltonian systems. *Arch. Rational Mech. Anl.*, 130(1):25–101, 1995. Communicated by P. Holmes.

[20] J. Hanson, J. Cary, and J. Meiss. Algebraic decay in self-similar markov chains. *J. Stat. Phys.*, 39(3):27–345, 1985.

[21] A. Katok and B. Hasselblatt. *Introduction to the Modern Theory of Dynamical Systems.*, volume 54 of *Encyclopedia of Mathematics and its Applications*. Cambridge University Press, 1995.

[22] G. Kovacic and S. Wiggins. Orbits homoclinic to resonances, with an application to chaos in a model of the forced and damped sine-gordon equation. *Physica D*, 57:185–225, 1992.

[23] L. M. Lerman. Isoenergetical structure of integrable Hamiltonian systems in an extended neighborhood of a simple singular point: three degrees of freedom. In *Methods of qualitative theory of differential equations and related topics, Supplement*, volume 200 of *Amer. Math. Soc. Transl. Ser. 2*, pages 219–242. Amer. Math. Soc., Providence, RI, 2000.

[24] L. M. Lerman and Y. L. Umanskiy. *Four-dimensional integrable Hamiltonian systems with simple singular points (topological aspects)*, volume 176 of *Translations of Mathematical Monographs*. American Mathematical Society, Providence, RI, 1998. Translated from the Russian manuscript by A. Kononenko and A. Semenovich.

[25] A. Litvak-Hinenzon and V. Rom-Kedar. Parabolic resonances in 3 degree of freedom near-integrable Hamiltonian systems. *Phys. D*, 164(3-4):213–250, 2002.

[26] A. Litvak-Hinenzon and V. Rom-Kedar. Resonant tori and instabilities in Hamiltonian systems. *Nonlinearity*, 15(4):1149–1177, 2002.

[27] A. Litvak-Hinenzon and V. Rom-Kedar. On energy surfaces and the resonance web. submitted preprint, 2003.

[28] D. W. McLaughlin and J. Shatah. Homoclinic orbits for PDE's. In *Recent advances in partial differential equations, Venice 1996*, volume 54 of *Proc. Sympos. Appl. Math.*, pages 281–299. Amer. Math. Soc., Providence, RI, 1998.

[29] J. Meiss. Symplectic maps, variational principles, and transport. *Rev. of Modern Phys.*, 64(3):795–848, 1992.

[30] N. N. Nehorošev. Action-angle variables, and their generalizations. *Trans. Moscow Math. Soc.*, 26:181–198, 1972.

[31] N. Nekhoroshev. An exponential estimate of the time of stability of near-integrable Hamiltonian systems. *Russian Math. Surveys*, 32(6):1–65, 1977.

[32] J. Pöschel. On elliptic lower dimensional tori in Hamiltonian systems. *Math. Z.*, 202:559–608, 1989.

[33] V. Rom-Kedar. Homoclinic tangles—classification and applications. *Nonlinearity*, 7(2):441–473, 1994.

[34] V. Rom-Kedar. Parabolic resonances and instabilities. *Chaos*, 7(1):148–158, 1997.

[35] S. Smale. Topology and mechanics. I. *Invent. Math.*, 10:305–331, 1970.

[36] G. M. Zaslavsky. Chaos, fractional kinetics, and anomalous transport. *Phys. Rep.*, 371(6):461–580, 2002.